Chapter 22

Integrating Seismic-velocity Tomograms and Seismic Imaging: Application to the Study of a Buried Valley

Femi O. Ogunsuyi[1] and Douglas R. Schmitt[1]

Abstract

The architectural complexity of a paleovalley ~350 m deep has been revealed by acquisition and conventional processing of a high-resolution seismic-reflection survey in northern Alberta, Canada. However, processing degraded much of the high quality of the original raw data, particularly with respect to near-surface features such as commercial methane deposits, and that motivated use of additional processing algorithms to improve the quality of the final images. The additional processing includes development of a velocity model, via tomographic inversion, as the input for prestack depth migration (PSDM); application of a variety of noise-suppression techniques; and time-variant band-pass filtering. The resulting PSDM image is of poorer quality than the newly processed time-reflection profile, thus emphasizing the importance of a good velocity function for migration. However, the tomographic velocity model highlights the ability to distinguish the materials that constitute the paleovalley from the other surrounding rock bodies. Likewise, the reprocessed seismic-reflection data offer enhanced spatial and vertical resolution of the reflection data, and they image shallow features that are newly apparent and that suggest the presence of gas. This gas is not apparent in the conventionally processed section. Consequently, this underscores the importance of (1) ensuring that primarily high-frequency signals are kept during the processing of near-surface reflection data and (2) experimenting with different noise-suppression and elimination procedures throughout the processing flow.

Introduction

Buried valleys are exactly what their name implies: valleys that have been filled with unconsolidated sediments and covered so that their existence is not apparent at the earth's surface. They are abundant in recently glaciated areas in North America and Europe (e.g., ÓCofaigh, 1996; Fisher et al., 2005; Hooke and Jennings, 2006; Jørgensen and Sandersen, 2008). Their internal structure is complex, with a heterogeneous mix of fluid-saturated porous and permeable sands and gravels mixed with low-porosity and low-permeability diamicts and clays.

Surface geologic mapping often cannot locate or delineate the extent of such buried valleys because they are masked at the surface by recently deposited glacial sediments; invasive methods such as boreholes have been employed to characterize them (e.g., Andriashek and Atkinson, 2007). Moreover, the physical properties of these glacially derived sediments often differ significantly from the surrounding bedrock into which the valleys had been cut; that contrast allows use of many complementary geophysical methods. Geophysical techniques also can provide laterally continuous information about the subsurface, so they might be preferred over intrusive methods.

Geophysical methods have been used widely to investigate near-surface targets (Hunter et al., 1984; Miller et al., 1989; Clague et al., 1991; Belfer et al., 1998; Nitsche et al., 2002; Benjumea et al., 2003; Sharpe et al., 2004; Chambers et al., 2006), and specifically, buried valleys (Greenhouse and Karrow, 1994; Jørgensen et al., 2003a; Jørgensen

[1]*Institute for Geophysical Research, Department of Physics, University of Alberta, Edmonton, Alberta, Canada. E-mail: ogunsuyi@phys.ualberta.ca; dschmitt@ualberta.ca.*

et al., 2003b; Steuer et al., 2009). In particular, refraction- and reflection-seismic methods have been used extensively in various glacial environments to image subsurface structures (e.g., Roberts et al., 1992; Wiederhold et al., 1998; Büker et al., 2000; Juhlin et al., 2002; Schijns et al., 2009) and to study buried valleys (Büker et al., 1998; Francese et al., 2002; Fradelizio et al., 2008). In such studies, seismic inversion often is limited to first-arrival traveltimes for the input (e.g., Lennox and Carlson, 1967; Deen and Gohl, 2002; Zelt et al., 2006), rather than inputting both refracted and reflected traveltimes (e.g., De Iaco et al., 2003).

The fresh groundwater within buried valleys is usually their most important resource. Consequently, in the last 15 years, numerous and varied geophysical investigations have been undertaken in northern Europe (e.g., Gabriel et al., 2003; Sandersen and Jørgensen, 2003; Wiederhold et al., 2008; Auken et al., 2009) and North America (e.g., Sharpe et al., 2003; Pullan et al., 2004; Pugin et al., 2009) to locate and define such features for their exploitation and protection. Further, the porous sands and gravels in buried valleys also can contain local biogenic gas (Pugin et al., 2004) or leaked thermogenic methane. Such gas sometimes exists in modest commercial quantities, but it also can be a significant safety hazard for drillers.

Ahmad et al. (2009) recently described an integrated geologic, well-log, direct-current electrical, and seismic-reflection study of one such large buried valley in northern Alberta, Canada. Using the same seismic data set, we extend Ahmad et al.'s (2009) work by exploring development of a seismic tomographic velocity model to characterize the paleovalley on the basis of the material/interval velocities. The model was generated by performing an inversion of the traveltimes of both refracted and reflected waves.

Refracted, guided, air, and surface waves are examples of source-generated noise (coherent noise) that presents considerable problems during seismic data processing (Büker et al., 1998; Montagne and Vasconcelos, 2006). Accurate separation of refracted and guided waves from shallow reflections is difficult, and such linear events can stack coherently on reflection profiles, causing misinterpretation (Steeples and Miller, 1998). Performing a noise-cone muting might prove useful in eliminating some of the source-generated noise, but reflections also are muted in the process (Baker et al., 1998). Surgical noise-cone muting was employed to remove the coherent noise in the previous study (Ahmad, 2006; Ahmad et al., 2009). Apart from the possibility that this procedure might not have removed the guided waves located outside the noise-cone zone on the shot gathers, it inadvertently also might have eliminated some true reflections during muting. Either way, the resulting seismic profile is not as satisfactory as one might expect from the quality of the raw shot gathers. Therefore, in our study, we instead performed radial and slant-stack noise-suppression procedures on the data set to retain and enhance shallow reflections that might have been removed by muting or masked by source-generated noise.

Because the dominant frequency of a seismic wave controls the separation of two close events (Yilmaz, 2001), our new processing scheme was aimed also at improving the spatial and vertical resolution of the data set because the seismic-processing sequence of the previous study did not account for adequately filtering out the low frequencies. We subsequently attempted to use the tomographic velocity model to perform a prestack depth migration (PSDM) after the noise-suppression strategies had been used on the data set. To our knowledge, PSDM algorithms and the radial and τ-p noise-suppression techniques that often are employed in more conventional and deeper petroleum exploration have not been applied to such near-surface seismic data.

The goal here is not to provide a new geologic interpretation of Ahmad et al.'s (2009) study, but instead to share the experiences gained in applying several tools, some of which to our knowledge have been employed heretofore only in deeper petroleum exploration. One special improvement over the earlier work is that this reprocessing has permitted imaging of shallow methane deposits within the glacial materials, and as such this work has implications for both resource exploration and safety enhancement for drillers.

Background

Details and maps of the location of the survey in the northwestern corner of Alberta, centered at approximately 58° 35′ N and 118° 31′ W, are found in Ahmad et al. (2009). The near-surface geology of northeastern British Columbia and northwestern Alberta has been studied extensively in the last decade (e.g., Best et al., 2006; Hickin et al., 2008; Levson, 2008). The surface geology of the area immediately over the profile has been investigated by Plouffe et al. (2004) and Paulen et al. (2005), and it is established to be blanketed primarily with glacial, lacustrine, and glaciolacustrine sediments of variable depths; those authors also have produced numerous complementary maps of the region's general surface geology.

A brief explanation of the bedrock geology is necessary to assist the reader's understanding of later geophysical responses. The consolidated bedrock sediments beneath

the Quaternary cover in the region lie nearly flat, and when they are undisturbed they consist of ~250 m of Cretaceous siliclastic sands and shales underlain, across a sharp unconformity (sub-Cretaceous), by more indurated Paleozoic carbonates and shales. Hickin et al. (2008) and references therein offer more detailed descriptions of the region's bedrock geology. Ahmad et al. (2009) also provide representative well logs that, to first order, approximately categorize the sediments on the basis of sonic velocity and density.

Seismic Field Program

A high-resolution 2D seismic profile was acquired over a survey length of approximately 9.6 km in an east-west direction (Figure 1). The seismic survey line straddles the surface over the large buried valley to the east and the out-of-valley region to the west, as determined from the maps of bedrock topography and surface geology (Plouffe et al., 2004; Paulen et al., 2005; Pawlowicz et al., 2005a, 2005b) (Figure 1). The purpose of the survey was to image the formation above the sub-Cretaceous unconformity and hence to delineate the buried channel and obtain important information about its internal structure.

A summary of the acquisition parameters is provided in Table 1. The P-wave seismic source used was the University of Alberta's IVI Minivib™ unit, operated with linear sweeps of a 7-s period, from 20 Hz to 250 Hz, at a force of approximately 26,690 N (6000 lb). The seismic traces were acquired with high-frequency (40-Hz) geophone singles (to attenuate some of the ground-roll noise) at a 4-m spacing using a 240-channel semidistributed seismograph that consists of 10 24-channel Geode™ field boxes connected via field intranet cables to the recording computer. Approximately five to eight sweeps per shotpoint were generated by the seismic source at a 24-m spacing. Cross-correlation of the seismic traces with the sweep signal (to generate a spike source), as well as vertical stacking, were carried out in the field. The final stacked records were saved in SEG2 format and later were combined with survey header information into a single SEGY format file for processing.

Generally, good coupling between the vibrator plate and the frozen, snow-covered ground was achieved, as determined by the constant nature of the force over time during the sweep period and by the transmission of high seismic frequencies (Ahmad et al., 2009). In a similar manner, there was good coupling between the ground and the geophones, which were frozen in place overnight, thus improving the signal-to-noise ratio (S/N). The average

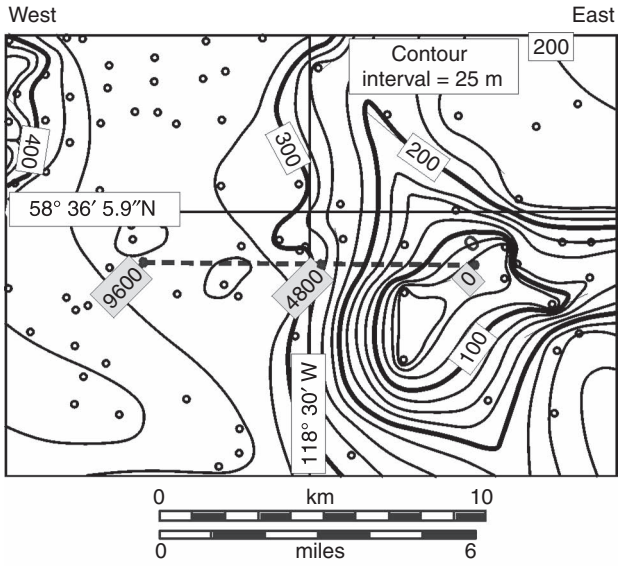

Figure 1. Contours of bedrock-topography elevation in meters above sea level (asl), with the location of the 2D survey line shown as a broken line. Black labels inside gray boxes indicate distance in meters from east to west, with the origin at 0 m. The small unfilled circles are wellbore locations used to generate the bedrock-topography map. After Pawlowicz et al. (2005a). Used courtesy of Alberta Energy and Utilities Board/Alberta Geological Survey.

Table 1. Acquisition parameters for the 2D seismic survey.

Parameter	Value
2D line direction	East-west
Length of profile	~9.6 km
Source	6000-lb IVI Minivib™ unit
Source frequency	20–250 Hz
Source type	Linear
Source length	7 s
Source spacing	24 m
Vertical stacks	5–8
Number of unique shotpoints	399
Receivers	40-Hz single geophones
Receiver spacing	4 m
Recording instrument	Geometrics Geode™ system
Number of channels	192–240
Sampling interval	0.5 ms
Record length	1.19 s
Nominal fold	~40

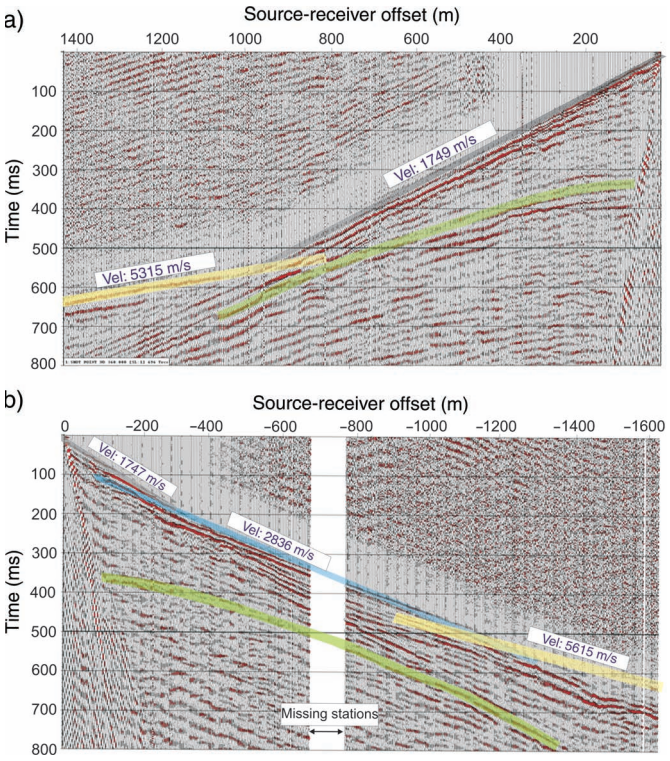

Figure 2. Raw shot gathers acquired at different locations on the survey line. The apparent velocities of different refractors, obtained from a simple intercept-time refraction method, are displayed. Positive-offset values are to the west of the respective shotpoint, whereas negative offsets are to the east. The gray highlight shows a direct wave through the Quaternary fill, the blue highlight is a refracted wave turning through the Cretaceous rock, the yellow line denotes the refracted wave through the Devonian, and the reflection from the top of the Devonian is in green. (a) An eastern shot gather (shotpoint 360) acquired over the valley on the seismic line. (b) A western shot record (shotpoint 1848) acquired outside the buried valley.

common-midpoint (CMP) fold for the survey was approximately 40. Two representative shot gathers from either end of the seismic profile (Figure 2) highlight the evolution of the traveltimes (and hence of velocity structure) from east to west.

Seismic Traveltime Inversion

A linearized traveltime-inversion procedure, developed primarily for modeling 2D crustal refraction and wide-angle data (comprehensively described in Zelt and Smith, 1992; and applied in Song and ten Brink, 2004), was used. The inversion incorporates traveltimes of the direct, refracted, and reflected events. The geometry of the model is outlined by boundary node points that are connected through linear interpolation, whereas the velocity field is specified by velocity value points at the top and base of each layer. The velocity within each block varies linearly with depth (between the upper and lower velocities in a layer) and laterally across the velocity points along the upper and lower layer boundaries.

Examination of the refracted events on the shot gathers offers an important insight into the apparent velocity structure of the survey line. Figure 2a shows a shot gather acquired at the east end of the profile immediately over the buried valley. Performing a simple intercept-time refraction analysis on this gather suggests that a simple two-layer model could be sufficient (see Ahmad et al., 2009). The wave passage through the top layer (gray highlight) might be linked to a lower material velocity of the Quaternary fill compared with the higher velocity of the Devonian carbonates (yellow highlight). The velocity of the Quaternary rock is expected to be much lower than that of the Paleozoic rocks because of its weak consolidation, which resulted from minimal overburden pressures. On the other hand, the shot gather obtained at the west end and outside of the buried valley indicates three layers (Figure 2b): (1) a direct wave (gray highlight) that passes through a thin low-velocity Quaternary rock, (2) a refracted event, of intermediate velocities, from the top of the Cretaceous rock, and (3) another wave, with higher velocities, refracted from the top of the Paleozoic.

The Vista® processing package (GEDCO, Calgary) was used to pick the traveltimes within the shot gathers of both the refracted and reflected arrivals. Approximately 72,000 traveltime picks were made from 143 shot gathers, and these were assigned an average error of $\pm$ 5 ms to account for far-offset ranges and large depths (Ogunsuyi et al., 2009). The program RayGUI (Song and ten Brink, 2004) was used for the forward modeling and inversion.

After a series of tests was conducted to determine the optimal initial model, the starting model chosen was constructed with six layers, with the velocities varying linearly in each layer. The starting model was made up of coinciding locations of velocity and boundary nodes, which were almost equally spaced laterally at a distance of about 330 m for the top of the second and third layers, and were spaced irregularly for the other layers. Short-offset ($<$100-m) direct arrivals were inverted in the first layer to account for the near-surface velocity variations and the relatively flat surface topography. The second layer was defined for the inversion of the rest of the direct waves (the gray highlights in Figure 2), which constituted the greater part of the seismic waves through the Quaternary deposits. The third layer was defined for the refracted events

turning through the Cretaceous rock (i.e., the blue highlight in Figure 2b), whereas the base of the fourth layer represented the waves that reflected prominently from the top of the sub-Cretaceous unconformity. Technically, the third and fourth layers are supposed to be one and the same, but they were separated to give a measure of the validity of the final tomographic model, as demonstrated by the degree to which the gap (in depth) between the base of the third layer and base of the fourth layer will be reduced subsequent to the inversion process. The refracted events (yellow highlights in Figure 2) through the Devonian rock were inverted for the fifth layer. A reflected event that could not be picked successfully for the whole length of the survey line was inverted for layer six, so less confidence is placed on the tomographic results at elevations below ~200 m below sea level.

The model was inverted layer by layer, from the top down, in a layer-stripping method intended to speed up and simplify the process (Zelt and Smith, 1992). This method involved the following steps: (1) simultaneously inverting the model parameters (both velocity and boundary nodes) of the topmost layer, (2) updating the model with the calculated changes, (3) repeating steps 1 and 2 until the stopping criteria are satisfied for the layer, (4) holding the model parameters of the layer constant for the subsequent inversion of all the parameters of the next layer in line, and (5) repeating steps 1 through 4 for all the other underlying layers in sequence. The uncertainties in the depths of the boundary nodes and velocity values were 10 m and 200 m/s, respectively.

The average values for the root-mean-square (rms) traveltime residual between the calculated and observed times for all layers was 16.4 ms after seven iterations. Notably, adding more model parameters generally reduces the traveltime residual, but it does so at the expense of reducing the spatial resolution of the final model parameters (Zelt and Smith, 1992). Subsequent to the inversion, the difference in depth between the bases of the third and fourth layers was reduced acceptably on the west but was not reduced adequately on the east end inside the valley area. Merging the third and fourth layers before the inversion scheme, however, produced low ray coverage, thus violating one of the conditions for choosing a final model. Consequently, the six-layer model was chosen as the optimal model for the subsurface of the area under investigation.

Processing of Seismic-reflection Data

Ahmad et al.'s (2009) earlier study involves a conventional 2D CMP processing scheme (Table 2) whereas the new processing sequence (adapted from Spitzer et al., 2003) followed in this study is complemented with noise-suppression procedures that involve transformation of time-space (*t-x*) data into other domains (Table 3). The motivation for designing a new processing scheme for the seismic data was the need to determine whether reflections were eliminated or degraded by the muting functions adapted in the previous study or were covered up by source-generated noise. If either was the case, we wished to recover the affected reflections and additionally to improve the lateral and vertical resolutions of the reflection profile.

Low-quality traces resulting from noisy channels, high amplitude, and frequency spikes are problematic to a final image. Starting with the data set that already has geometry information assigned, the bad traces, with abnormally high amplitudes and frequencies, were identified by computing amplitude and frequency statistics on all the traces and

Table 2. Previous seismic processing sequence, as performed by Ahmad et al. (2009).

Processing step	Parameters
Geometry	—
Editing of bad trace	—
Offset limited sorting	–500 m to –12 m and 12 m to 500 m
Surgical mute	Auto bottom mute; manual surgical mute
CMP sorting	4-m bin size
Velocity analyses	—
NMO corrections	15% stretch mute
Elevation/refraction statics corrections	400-m asl datum; 1500 m/s replacement velocity
Residual statics corrections	Stack power algorithm
Inverse NMO corrections	—
Final velocity analyses	—
NMO corrections	15% stretch mute
Final residual statics corrections	Stack power algorithm
CMP stack	—
Band-pass filtering	45 to 240 Hz
Mean scaling	—
f-x prediction	—
Automatic gain control	150 ms

subsequently were removed. To adjust for the lateral changes in the thickness and velocity of the shallow depths and for the small elevation variations of sources and receivers, elevation/refraction statics corrections were conducted. A model of the shallow subsurface was established by inverting the first-break picks. Using a weathering velocity of 500 m/s, the average velocity of the first refractor was approximately 1700 m/s. The computed statics corrections were applied to a flat datum of 385 m above sea level, which was slightly above the highest elevation of the survey line. Total elevation/refraction statics corrections ranged from approximately −6.5 ms to +21 ms.

Table 3. Time-processing sequence for the 2D seismic survey.

Processing step	Justification
Trace editing	Removal of spurious traces
First-break picking	
Elevation/refraction statics corrections	Correction for shallow lateral variations
Spiking deconvolution	Compression of wavelet
Time-variant band-pass filtering	Suppression of low-frequency noise
Trace equalization	
CMP binning	
Initial velocity analyses	Determination of stacking velocities
NMO corrections	
Residual statics corrections	Correction for near-surface velocity changes
Inverse NMO corrections	
Radial domain processing	Removal of guided waves
Linear τ-p processing	Suppression of source-generated noise
Predictive deconvolution	Elimination of multiples
Dip-moveout (DMO) corrections	Preservation of conflicting dips
Final velocity analyses	Determination of stacking velocities
Final residual statics corrections	Correction for near-surface velocity changes
NMO corrections	
CMP stack	
f-x prediction	Reduction of incoherent noise
2D Kirchhoff time migration	Placing reflections in their true positions

Predictive deconvolution was not successful in removing some of the multiples in the data at this stage, so it was carried out in later processing. To compress the wavelet to a spike and thereby to increase the temporal resolution, spiking deconvolution was applied. After testing with different operator lengths for optimal results, a 20-ms operator length finally was employed. Low frequencies in the amplitude spectrum of the seismic data were dominated by direct and surface waves, but application of a low-cut frequency filter to the data set for the purpose of suppressing the noise might also inadvertently remove some deeper reflections that are characterized by low frequencies. To avoid this, time-variant band-pass filtering was applied to the data (80–300 Hz for a 0- to 380-ms time interval and 65–150 Hz for a 380- to 800-ms interval).

In addition, the band-pass-filtering step provides a means of enhancing temporal resolution of the seismic profile. Following the spiking deconvolution step, the amplitude spectra of the shot gathers were equalized adequately. To appreciate the value of these processing steps, a raw shot gather (shot-point number 660), affected by surface waves after elevation/refraction statics corrections (Figure 3a) and after application of spiking deconvolution, band-pass filtering, and trace equalization (Figure 3b), is displayed for comparison. Although most of the source-generated noise has not been eliminated, most of the surface waves have been suppressed and the reflection wavelet improved. Moreover, this processing step appears to have exposed additional guided waves that were concealed in the initial shot gather (Figure 3b). Details about the properties of these common seismic arrivals, which form the basis of our interpretation, can be found in Robertsson et al. (1996) and in Yilmaz (2001).

Choosing the best possible CMP bin size is imperative for minimizing spatial aliasing when one is processing seismic data for moderately to steeply dipping reflections (Spitzer et al., 2003). To determine the maximum CMP bin size b to use (Yilmaz, 2001), we evaluated

$$b \leq \frac{V_{\min}}{4 f_{\max} \sin\theta}, \tag{1}$$

where $V_{\min}$ is the minimum velocity, $f_{\max}$ is the maximum frequency, and θ is the maximum expected dip of structures. We arrived at a value of 3 m as the appropriate bin size for our data. Initial velocity analyses to determine the stacking

velocities were carried out on CMP supergathers by creating a panel of offset sort/stack records, constant-velocity stacks, and semblance output.

Residual statics are needed to correct for short-wavelength changes in the shallow velocity underneath each source-and-receiver pair. Surface-consistent residual statics by a stack power-maximization algorithm (Ronen and Claerbout, 1985) were estimated from the data after applying normal-moveout (NMO) corrections on the basis of the initial velocity analyses. The resulting average time shifts

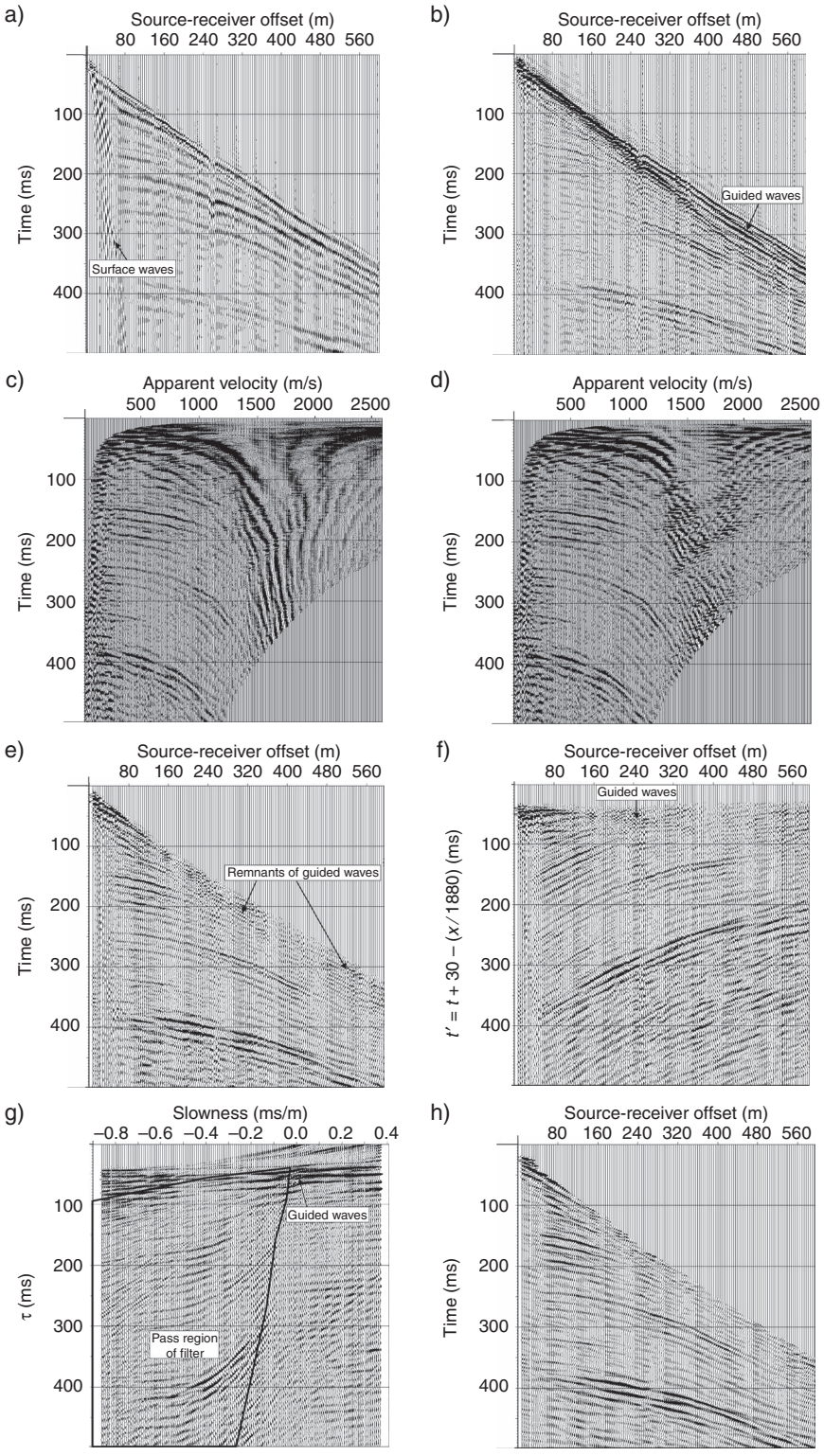

Figure 3. (a) A typical raw shot gather (shotpoint number 660) after elevation/refraction static corrections. (b) The same shot gather as in (a), after spiking deconvolution, time-variant band-pass filtering, and trace equalization. (c) The same shot gather as in (b), but after transformation to the *r-t* domain. (d) The same shot gather as in (c), after applying a low-cut filter of 45 Hz to suppress the linear events. (e) The same shot gather as in (d), after radial processing that involved transforming the shot gather from *r-t* to *t-x* coordinates. (f) The same shot gather as in (e), except that the time axis is reduced: traveltimes $t' = t + 30 - (x/1880)$, where 1880 m/s is the average velocity for the first arrival (as obtained from intercept-time refraction analyses). (g) The same shot gather as in (f), after linear τ-p transformation. The pass region of the τ-p filter is shown by a solid black line. (h) Result of linear τ-p processing obtained from filtering (g) and applying the inverse τ-p transformation. The records were scaled in relation to the rms amplitude of their respective gathers.

of about 4 ms were applied subsequently to the inverse NMO-corrected data.

As was noted earlier, most of the source-generated noise was not eliminated by band-pass filtering. Linear events (e.g., guided waves), which can affect the interpretation of shallow seismic adversely if they are not suppressed, still can be observed (Figure 3b). Some of this coherent noise can be reduced by mapping the data from a normal t-x domain into an apparent-velocity versus two-way-traveltime (radial or r-t) domain. The basis of this noise-attenuation process is that linear events in the t-x gather transform into a relatively few radial traces, with apparent frequencies shifting from the seismic band to subseismic frequencies (Henley, 1999). After transformation to the r-t domain (Figure 3c), a low-cut filter of 45 Hz was applied to the radial traces (Figure 3d) to eliminate the coherent noise mapped by an r-t transform to low frequencies. Subsequently, the data were transformed back to the t-x domain (Figure 3e). With regard to removal of some of the guided waves, the improvement of the data passed through radial processing (Figure 3e) compared with the quality of the original (Figure 3b) is quite noticeable.

To further reduce the source-generated noise (direct waves, surface waves, and remnants of guided waves) in the data, linear time-slowness (τ-p) processing was applied next. Linear and hyperbolic events in the t-x domain are mapped into points and ellipses, respectively, in the linear τ-p (or slant-slack) domain during linear τ-p transformation (Yilmaz, 2001). Hence, it is possible to separate these events in slant-slack gathers, to facilitate noise suppression. The steps involved in the linear τ-p processing are outlined below (modified from Spitzer et al., 2001).

1) The shot gathers were converted to reduced-traveltime format (linear-moveout terms) using velocities derived from intercept-time refraction analyses. To generate the gathers,

$$t' = t + 30 - (x/V_{\text{av}}) \qquad (2)$$

was applied to each trace, where t' is the reduced time in milliseconds, t is the original time in milliseconds, x is the source-receiver offset in meters, and V_{av} is the average velocity in kilometers per second. Generally, the average velocities change across the survey line. A bulk shift of 30 ms was applied to the data to accommodate possible overcorrections of linear moveout. As seen in Figure 3f, the first arrivals and related source-generated noise have been converted to horizontal or nearly horizontal events.

2) Because the recording direction is not preserved during τ-p mapping (Spitzer et al., 2001), we separated the positive source-receiver offsets from negative offsets before processing them further.

3) The reduced-traveltime shot gathers were transformed into the linear τ-p domain using a range of p (slowness) values from -0.9 to 0.4 ms/m for positive offsets and -0.4 to 0.9 ms/m for negative offsets, to exclude surface waves and other low-velocity coherent noise, and with τ being intercept time. Although minor aliasing of the surface waves was observed in the slant-stack gathers (as observed in the frequency-wavenumber or f-k domain) of the data, it does not seem to pose a major problem to our data.

4) The reflected events (i.e., ellipses) in the τ-p domain are quite distinguishable from the source-generated noise (mapped to points around $p = 0$ ms/m). We defined a 2D pass filter (as illustrated in Figure 3g) around the elliptical events for data on each side of the split source-receiver offset, and we set the amplitudes of the regions outside the area to zero. A 5-ms taper was applied in the τ direction to the data, to minimize artifacts.

5) We then performed inverse linear τ-p transformation on the filtered τ-p data. Subsequently, the data for the positive and negative offsets were recombined, and the linear moveout terms and the time bulk shift were removed. The results show that most of the linear source-generated noise has been reduced with no adverse effect on the reflections (Figure 3h).

Some linear events still remain in the data. This could be because spatially aliased events in the t-x domain might spread over a range of slowness values, including the pass region of the filter, in the τ-p domain (Spitzer et al., 2001). These remnant linear events were removed carefully by surgical muting. Applying predictive deconvolution with 150-ms operator length and a prediction distance of 15 ms at this stage appeared to remove some of the multiples at greater depths.

Stacking velocities are dip-dependent, so in the case of an intersection between a flat event and a dipping event, one can choose a stacking velocity in favor of only one of these events, not both (Yilmaz, 2001). Dip-moveout (DMO) correction preserves differing dips with dissimilar stacking velocities during stacking. We applied DMO corrections to the NMO-corrected gathers (using velocities from the initial conventional CMP velocity analyses) and then performed an inverse NMO on the resultant data. Subsequently, a final velocity analysis was carried out on CMP supergathers (made up of 15 adjacent composite CMPs). The stacking velocities of the τ-p-processed and DMO-corrected data can be picked with greater assurance compared with the

data that were not passed through those processing steps. The final stacking velocities from conventional CMP velocity analyses (Figure 4a) and the corresponding interval velocities after conversion (Figure 4b) show the lateral variation in the velocities from the buried valley to the Cretaceous bedrock, as does the result of the tomographic inversion (Figure 4c).

Using statics estimates that were computed after NMO corrections based on the final stacking velocities had been done, residual statics again were carried out. As a result of NMO correction, a frequency distortion occurs, particularly for shallow events and large offsets (Yilmaz, 2001). A stretch mute of 60% was applied to the data to get around that problem. The data later were stacked and frequency-space (f-x) prediction was performed on the data to reduce incoherent noise (Canales, 1984). For display purposes, an automatic gain control of 300 ms was applied to the final stacked section (Figure 5a). To place the reflections in the true subsurface positions, 2D Kirchhoff poststack time migration also was performed on the seismic data (Figure 5b).

Although it is possible to make an interpretation about the structure of the buried valley from the time-stack section, correlation with depth values cannot be made without having a time-depth relationship. We conducted a simple depth conversion of the seismic section, using average velocities from the generated tomographic model and from conventional CMP velocity analyses. However, the results showed a prominent reflection (the sub-Cretaceous unconformity) being pulled down substantially at the west end of the profile. This probably is the result of the considerable lateral variation in velocity. Instead, prestack depth-migration (PSDM) processing was performed on the data, after the noise-suppression procedures (as outlined in Table 4), by using the velocity distribution derived from the traveltime tomography of refracted and reflected events

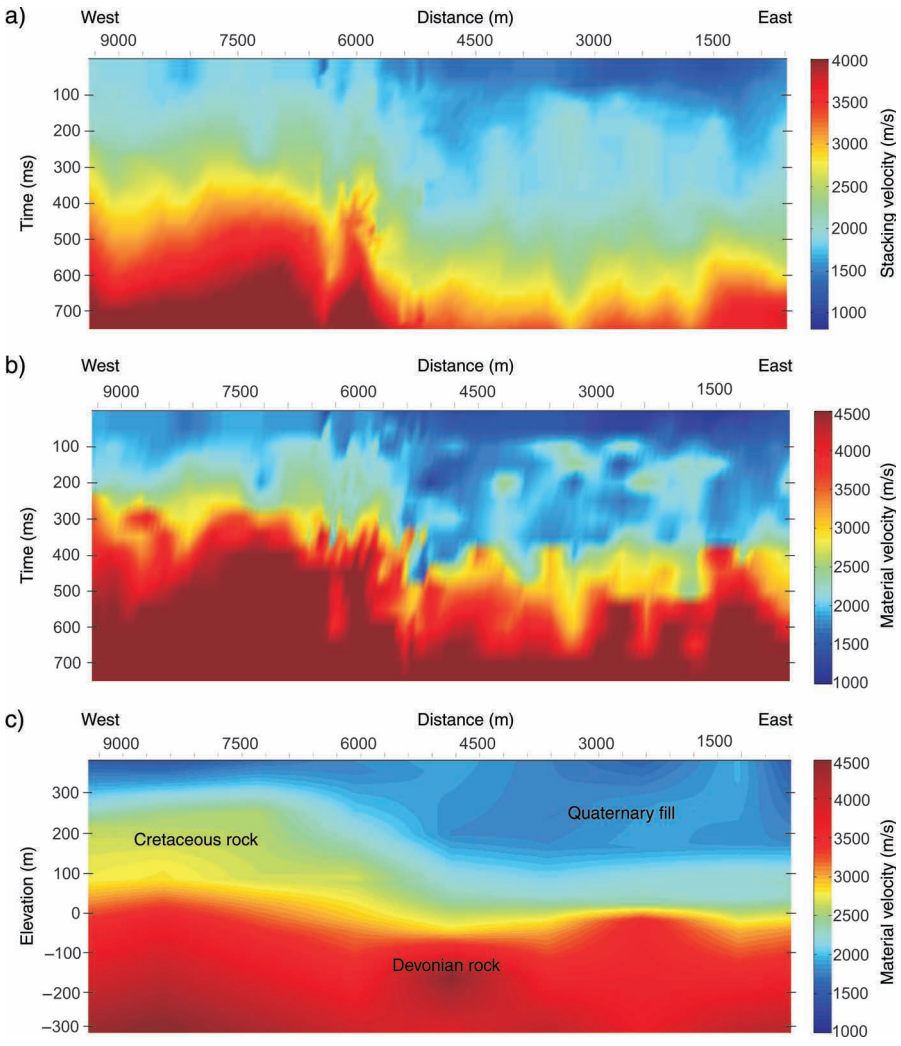

Figure 4. (a) Final stacking velocities as picked during traditional velocity analyses on CMP supergathers. The vertical axis is two-way time in milliseconds. (b) for the same data as in (a), after conversion to interval velocities. (c) The interval velocities of the subsurface, as acquired from the traveltime inversion with a vertical exaggeration of about five. The vertical axis is elevation (m) above sea level (asl). The different rock bodies, as labeled, can be distinguished on the basis of their respective material velocities.

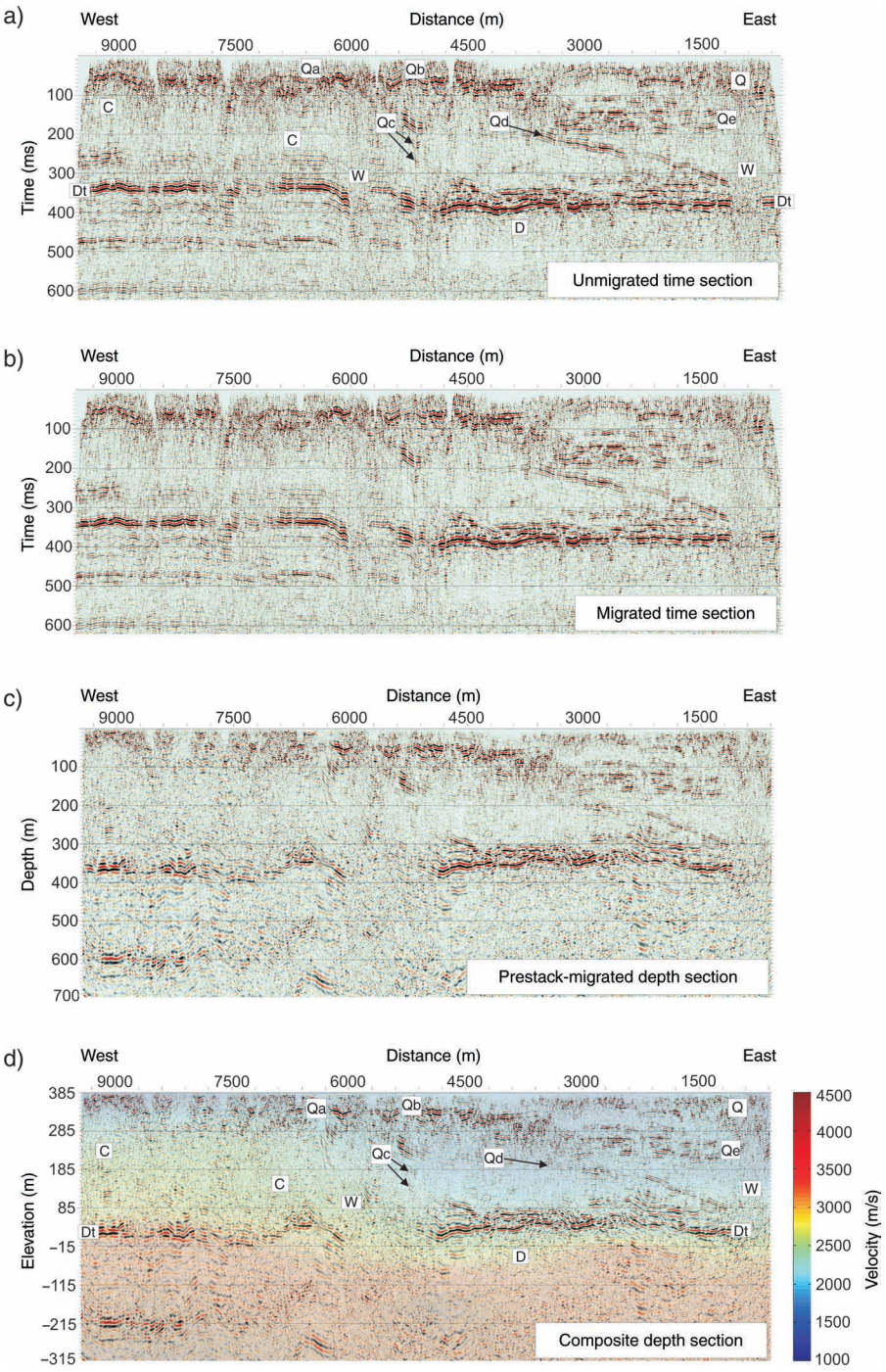

Figure 5. (a) Unmigrated time seismic profile with interpretative tags. (b) Post-stack time-migrated seismic section. (c) Final prestack depth-migrated seismic. (d) The same data as in (c), overlaid here with the traveltime inversion velocities. The interpretation tags in (a) and (d) are D: Devonian rock; C: Cretaceous rock; Q: Quaternary fill; w: washed-out regions; Dt: top of Devonian unconformity horizon; Qa: possible top of Cretaceous bedrock; Qb: strong Quaternary event with possible gas presence; Qc: Quaternary dipping reflectors; Qd: strong dipping event in the Quaternary; and Qe: flat-lying reflectors in the Quaternary fill. An automatic gain control of 300 ms was applied to each of the stacked seismic images and they were scaled in relation to the mean amplitude of their respective section.

(Figure 4c). Although the results from the PSDM procedure showed poorer quality than had been expected, the depth to the prominent reflector at the top of the unconformity agrees acceptably with available wellbore information. The resulting PSDM image obtained with a split-step (Stoffa et al., 1990) shot-profile (Biondi, 2003) migration algorithm is displayed on its own (Figure 5c) and is overlaid with a velocity field from traveltime tomography and some interpretation tags (Figure 5d).

Results and Discussion

The tomographic velocity distribution of the subsurface (Figure 4c) that was created from inversion of refracted and reflected traveltimes is an improvement over the simple refraction analysis carried out in the previous study. Delineating the paleovalley on the basis of differences in the material velocities of the rocks in the area is the foremost reason for generating the tomography. The Quaternary

sediments in the east are distinguished readily from the Cretaceous bedrock in the west with material velocities, which vary from ~1700 m/s in the buried valley to ~2800 m/s in the bedrock (Figure 4c). This is not surprising because the Quaternary-fill deposits are expected to be loosely consolidated (thereby giving rise to lower compressional-wave velocities) compared with the stiffer Cretaceous bedrock. Accordingly, the edge of the valley is defined by rapid changes in the material velocities, as can be observed in the inversion result at distances between 4800 and 6000 m. Vertically, the transition in the velocities from the inversion (Figure 4c) is not abrupt, but the geologically sharp unconformity (see Ahmad et al., 2009) at the base of both the Cretaceous and Quaternary sediments still is noticeable. The velocities rise rapidly in the tomographic result to values >3500 m/s, which is typical of the deeper Devonian carbonates. The stacking velocities that were converted to interval velocities (Figure 4b) are comparable to the final material velocities derived from the results of the traveltime inversion (Figure 4c). The similarities, both in magnitude and features, between the two velocity images (Figure 4b and 4c) are apparent.

However, it is noteworthy that the edge of the valley (at an approximate distance of 5700 m), as deduced from the interval velocities (Figure 4b) derived from the picked stacking velocities, appears more abrupt than is observed in the tomographic velocity model (Figure 4c). This difference in velocity transition from the valley to the Cretaceous rock could be related to challenges encountered in the course of picking the stacking velocities on washed-out CMP supergathers, because reflections were difficult to detect in the washout zones.

It also is observed that the top of the sub-Cretaceous unconformity (Ahmad et al., 2009), which is characterized by a noticeable jump in velocities, appears to be more uneven in the converted velocities (Figure 4b) than in the results of the traveltime inversion (Figure 4c). Minor errors in the stacking-velocity picking could account for that contrast. It is clear that the tomographic data are successful in delineating the paleovalley.

However, the low-resolution inversion results (Figure 4c) could not image details of the structure within the valley that are evident in the reflection profiles (Figure 5a and 5b). Some of the features include a variety of dipping reflectors Qc at the edge of the valley; a strong, dipping reflector Qd that is unconformable with the other reflectors; and the numerous flat-lying reflectors Qe. Nonetheless, because of inadequate well information within the valley area, we cannot ascertain whether substantial material-velocity differences exist in the various sediments that constitute the buried valley. Further, if there are material-velocity differences, we are not sure whether they can be observed clearly on sonic logs.

Table 4. PSDM processing sequence for the 2D seismic survey.

Processing step
Trace editing
First-break picking
Elevation/refraction-statics corrections
Spiking deconvolution
Time-variant band-pass filtering
Trace equalization
CMP binning
Initial velocity analyses
NMO corrections
Residual statics corrections
Inverse NMO corrections
Radial domain processing
Linear τ-p processing
Predictive deconvolution
Final velocity analyses
Final residual statics corrections
Prestack depth migration using tomographic velocity model
Stack
f-x prediction

To convert the time section to depth, we used the tomographic velocity model to perform a PSDM on the data (Figure 5c and 5d). The quality of the results, however, was not as good as anticipated, as can be observed from the degraded reflection continuities, mostly in the western part of the line (i.e., distances > 5000 m). This could be related to minor problems in the velocity model, which for improved results might require iterative refinement with the aim of serving as input to the PSDM algorithm (see Bradford and Sawyer, 2002; Morozov and Levander, 2002; Bradford et al., 2006). Seismic anisotropy also might play a role here because the tomographic image, which includes refracted head and turning waves, could be biased by these more horizontal propagation paths. In addition, because a 2D migration can only collapse the Fresnel zone in the migration direction (Liner, 2004), the discontinuous nature of the reflections in the PSDM data

could result from the fact that we are imaging an irregular 3D structure into the 2D profile.

Most of the wellbores in the immediate vicinity of the 2D line are for shallow gas production; hence, they are not deep enough to reach the top of the unconformity. Nonetheless, two wells to the south at a distance of <3 km from the survey line penetrated the unconformity at an elevation of about 28 m above sea level, which is approximately 7 m deeper than the depth to the unconformity that is clearly observable on the PSDM image (Figure 5d). Considering the uneven topography on top of the unconformity (Figure 5a), this minor discrepancy in depth is not unreasonable. However, uncertainty is involved in estimating the top of the unconformity — which is known from core and well logs to be abrupt — using the "smeared" results of the traveltime inversion. As mentioned earlier, the initially separated third and fourth layers of the tomographic velocity model are supposed to be one and the same. However, subsequent to the inversion they were merged adequately only for the western part of the profile line and not for the eastern side (i.e., for the distance of 1200 to 5100 m, see the section on seismic traveltime inversion). Hence, either the top or the base of the fourth layer can be picked as the top of the unconformity. If the top of layer four is selected as the top of the unconformity, the results of the traveltime inversion and the PSDM stacked section agree, but if the base of layer four is picked, a depth discrepancy of approximately 43 m occurs. In addition, estimating the depth of the unconformity from the tomography, on the basis of an interpretation of the colors, is quite subjective and easily biased.

The result of the reflection data processed previously using conventional steps (without radial and linear τ-p processing) (Ahmad et al., 2009) is displayed in Figure 6a, and the result from the processing steps presented in this con-

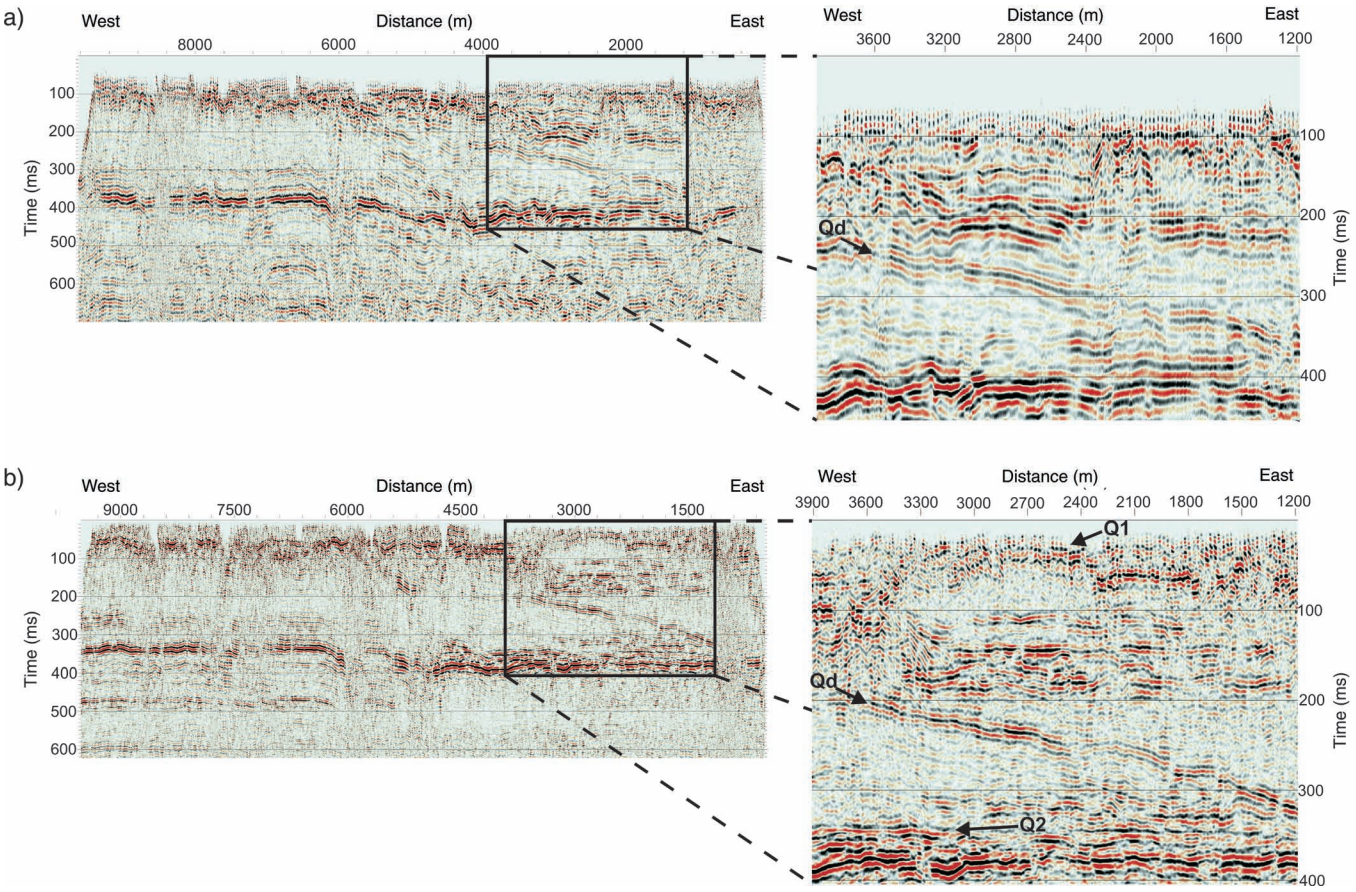

Figure 6. (a) A seismic section processed previously using conventional processing steps (Ahmad et al., 2009) and not optimized to reduce source-generated noise. (b) Newly processed seismic section, optimized to reduce noise. An automatic gain control of 300 ms was applied to both stacked seismic sections and they were scaled with respect to the mean amplitude of the respective section. The images on the right-hand sides are magnified to highlight better resolution of the newly processed reflection seismic profile. The interpretation tags are: Qd: strong dipping event within the Quaternary; Q1: shallow event within the Quaternary; and Q2: resolved Quaternary horizons lying above the Devonian.

tribution is shown in Figure 6b for comparison. In the magnified images beside each profile, better temporal and lateral resolution in the newly processed seismic is observed. Using the quarter-wavelength limit of vertical resolution (Widess, 1973) and a velocity of 2000 m/s, a vertical resolution of 16.6 to 6.25 m was obtained for the previously processed seismic data, from dominant frequencies typically ranging from 30–80 Hz.

Similarly, a vertical resolution of 10 to 3.3 m was obtained for the newly processed seismic profile, from dominant frequencies primarily in the 50- to 150-Hz range. Evaluating the equation for the threshold of lateral resolution — i.e., for the radius of the first Fresnel zone (Sheriff, 1980) — with 1000 m/s as velocity at 150-ms two-way traveltime, the lateral resolution of the seismic section from the previous study ranged from 35.4 to 21.6 m (30- to 80-Hz dominant frequencies). That of the new seismic profile ranged from 27.4 to 15.8 m (50- to 150-Hz dominant frequencies) at about the same two-way traveltime. Thus, it is evident from these values that the resolution of the data has been enhanced in the new seismic profile.

It is unclear from the previous seismic profile (Figure 6a) whether the low-amplitude horizons immediately below strong, dipping event Qd are flat lying or at an incline. On the other hand, the new profile (Figure 6b) shows clearly that the above-mentioned horizons dip from west to east. Clarification of the dipping nature of these events was perhaps a result of the improved resolution of the new data, but one cannot rule out the possibility that the new processing scheme recovered some eliminated parts of the reflections. Those parts could have been removed by the mute functions used in the previous processing, thus making them less coherent. At the distance of about 2400 to 3000 m and the time 30 ms, it also is possible to identify a nearly horizontal feature Q1 on the new seismic data (Figure 6b).

To avoid misinterpreting as reflections what really are coherent events and artifacts from various processing steps for enhancement (e.g., Steeples and Miller, 1990; Steeples et al., 1997; Sloan et al., 2008), we attempted to validate the true nature of the Q1 feature directly from the filtered shot records (Figure 7a). However, this shallow feature exhibited a lower frequency than did deeper reflections on shot gathers, and it could not be correlated with certainty to any true reflection. Thus, without additional supporting evidence, the Q1 feature cannot be considered to be any more than a stacked coherent event.

Clearly noticeable on the new seismic profile (Figure 6b), between distances 3000 and 4200 m, are horizons Q2, lying directly on top of the unconformity. On the old seismic section (Figure 6a), these horizons appear to be merged with the sub-Cretaceous unconformity and cannot

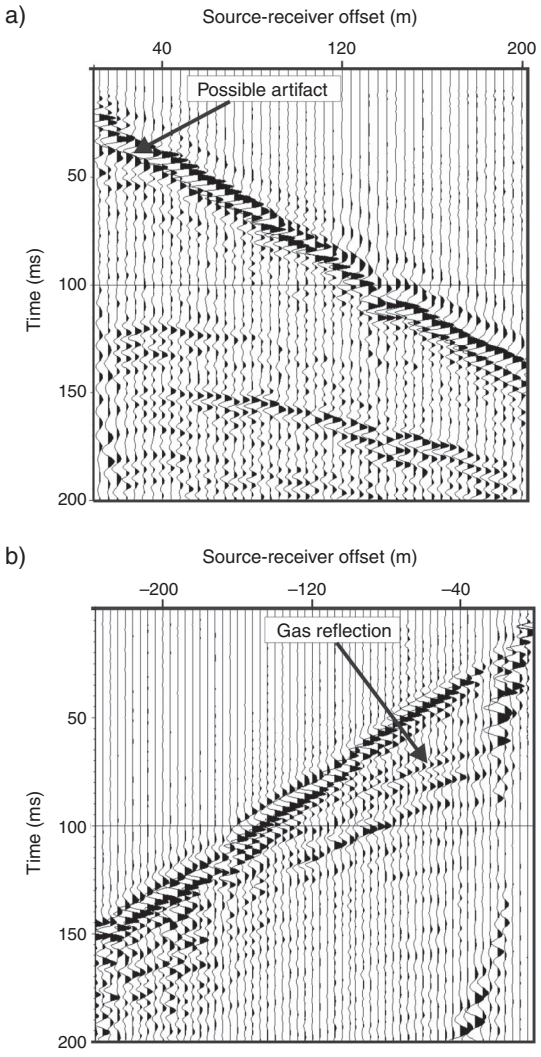

Figure 7. Raw shot gathers after elevation/refraction static corrections, spiking deconvolution, time-variant band-pass filtering, and trace equalization, located near (a) the poorly constrained shallow, 30-ms Q1 feature from Figure 6b, and (b) a strong reflection that is interpreted to be the top of a near-surface methane-saturated sand shown in Figure 8b.

be distinguished easily. On the new profile, these high-amplitude reflections seem to cover almost the entire extent of the bottom of the valley, from distance 4200 m on the west to distance 1200 m on the east — at which point they become incoherent because of the smeared zone. Considering the fact that these flat-lying reflectors were not observed outside the paleovalley (distances >6000 m), they are likely Quaternary sediments that were deposited immediately after the erosion caused by glacial meltwaters; alternatively, they might be remnants of the erosion of the valley itself.

Washout/smeared zones were problematic to the imaging (Figure 5). In particular, the western edge of the

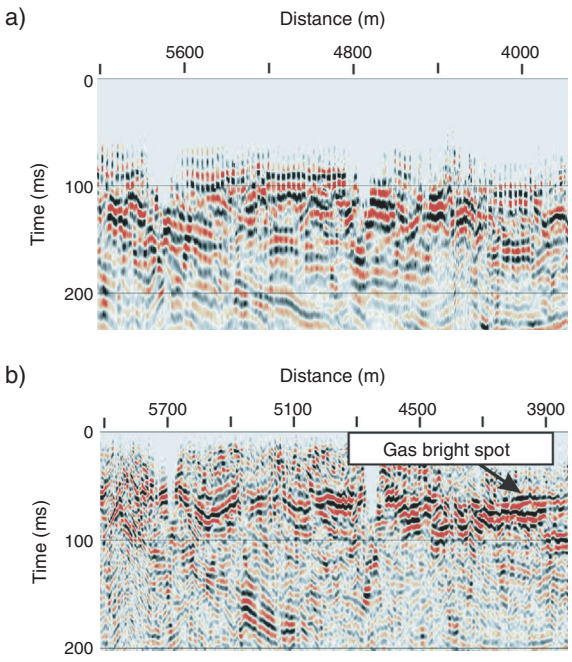

Figure 8. Detailed comparison of the topmost section of a profile over a known near-surface gas reservoir. (a) The previously processed seismic section of Ahmad et al. (2009), and (b) the reprocessed seismic-reflection profile, showing a strong reflector that indicates the presence of free gas.

valley (at approximately distance 5700 m) was not well imaged because of a large washout zone at that location. The washout zones are attenuated regions where continuous reflections are not observed. As can be seen from the unprocessed shot gathers, it is not possible to make out any strong reflections in these zones. Although the exact cause of this attenuation is not known, it likely is associated with thicker zones of muskeg (bogs filled with sphagnum moss). The most conspicuous event in the reflection sections is the strong reflector Dt located approximately halfway down the vertical axis of the profiles. Aside from the washout zones W, this reflector, which is the unconformity above the Devonian rock, spans the entire survey line. Above the unconformity lie Cretaceous bedrock C to the west of distance 6000 m and Quaternary sediments Q to the east of distance 4800 m. The edge of the paleovalley, dipping from west to east, lies between distances 4800 and 6000 m.

There is a shallow high-amplitude reflection Qa from approximately distance 6000 to 9300 m at a two-way traveltime of ~50 ms (Figure 5a). This event could be the top of the Cretaceous bedrock. It is interesting to note that the reflection is not continuous across the entire survey line to the valley area on the eastern side. A possible explanation for this could be the minimal impedance contrast between the glacial sediment that blankets the whole area and the deposits that constitute the buried valley. This event could not be seen clearly on the previously processed seismic profile, which points to the fact that the new data are improved relative to the old.

Shallow features that were not apparent in Ahmad et al.'s (2009) previous processing (Figure 8a) now are visible in Figure 8b and are particularly noteworthy. As also can be seen on the PSDM seismic profile (Figure 5d), there is a strong reflector Qb at an elevation of approximately 345 m above sea level (at an ~40-m depth), inside but at the edge of the valley (between distances 3900 and 5100 m). This strong reflector, also clearly visible in the raw shot gathers (e.g., Figure 7b), likely indicates the presence of free gas. Such gas has been produced in commercial quantities from this site (Rainbow and Sousa fields in northern Alberta) in the last decade, at depths of less than 100 m (see Pawlowicz et al., 2004; Kellett, 2007), and it still is being produced. Considering that the shallow gas in the Rainbow field has a chemical signature that indicates a deeper, thermogenic origin and given the high electrical resistivities recorded in our survey area, it has been suggested that gases migrated from the Cretaceous bedrock formations and were trapped in the porous Quaternary sediments (Ahmad et al., 2009).

These shallow gas deposits had been found serendipitously during previous drilling of shallow water or deeper petroleum boreholes, and on numerous occasions they have led to dangerous releases of flammable methane gas that sometimes have destroyed rigs. Ground-based electrical-resistivity tomography (ERT) studies have been used in the past to indicate free, dry gas on the basis of high electrical resistivities. However, separating gas-saturated zones from freshwater-saturated zones can be difficult. The result of reprocessing this current data set suggests that with sufficient care, such shallow gas-filled zones can be distinguished. Conducting high-resolution seismic surveys over areas already targeted for drilling on the basis of ERT could add confidence and warn drillers about potential shallow blowout hazards.

Conclusions

We have presented the results of reanalyses of a near-surface seismic data set acquired over a paleovalley in northern Alberta, Canada. Our study includes (1) generation of a traveltime inversion to better delineate the buried valley, (2) reprocessing of the reflection data to enhance their resolution and recover any muted or degraded horizon from the previous processing, and (3) employment

of prestack depth migration, using velocities generated from the traveltime inversion, to obtain proper presentation of the data in depth scale.

Construction of tomographic velocity from inversion of direct, refracted, and reflected waves aimed to determine accurate representation of the velocity distribution of the area over the buried valley. That accomplishment would be an improvement over the results of the simple refraction analysis performed in the previous study. The results from the traveltime inversion show clearly that on the basis of the material velocities, a buried valley can be delineated from the surrounding rock bodies. The interval velocity of the loosely consolidated Quaternary-fill valley was observed to be approximately 1700 m/s, whereas that of the more competent Cretaceous bedrock was approximately 2800 m/s; the edge of the valley was defined by rapid changes in the material velocities. The interpretation made from the tomographic model is important because of the significant knowledge it provides about velocity contrasts of different materials. On the other hand, such detailed information about exact contrasts in the physical properties that produce reflections might not be deduced readily from seismic-reflection profiles alone, particularly given the absence of appropriate sonic and density well logs in the area. It is noteworthy, however, that the resolution of the traveltime inversion was insufficient to image the different rock features within the valley clearly, perhaps because of the structural complexities of the valley. It is suggested that waveform inversion with the tomographic results as the input model might be a viable option in imaging a paleovalley with complex architecture.

The seismic-reflection data were processed with a strategy optimized to enhance the lateral and vertical resolutions of the profile. An additional goal was to recover any muted or degraded reflection from the old study by employing noise-suppression techniques in other domains as opposed to the total muting of the noise cone in t-x coordinates. The processing steps included radial and linear τ-p processing used to reduce noise, and time-variant band-pass filtering to improve resolution.

Better resolution and more continuous events characterize the final stack of the newly time-processed reflection profile, compared with the previously processed seismic. The new seismic had lateral resolution enhanced by $\sim$30% in the near surface and vertical resolution enhanced by $\sim$75%. In addition, the dipping nature of some events, which could not be established on the initial processing, was ascertained on the new seismic images. Likewise, some indistinguishable horizons lying immediately over the sub-Cretaceous unconformity were identified on the newly processed profile. This underscores the significance of ensuring that primarily high-frequency signals are kept during the processing of near-surface reflection data.

Newly visible bright near-surface features, indicating the presence of gas, were imaged better in the new section. These features, which were not apparent in the old image, probably were muted during the previous processing sequence. Thus, we emphasize the importance of experimenting with different noise-suppression procedures before resorting to total muting of the noise cone. Aside from some washout zones in the data, the rock fabric and complex architecture of the channel and of the surrounding rock were imaged with better resolution in the newly processed stacked time section, and thus such processing is considered to produce a better result compared with that of the previous study.

Subsequently, we attempted a prestack depth migration on the noise-suppressed reflection-seismic data set, using the velocity field derived from the tomography. The quality of the result was poorer than we expected, with obvious reflection-continuity losses in some areas. We judged that problems in the tomographic model might be the reason for this. Refining the tomographic image iteratively as input into the PSDM algorithm might produce an image with unbroken reflections. The results, however, validate the importance of using a good velocity model for migration, and they underscore the challenge in obtaining the essential velocity accuracy from the shallow part of seismic data. In spite of the loss in reflection continuity, the depth to the sub-Cretaceous unconformity, as observed on the PSDM data, is consistent with the depth information obtained from two wellbores at distances of less than 3 km from the 2D seismic profile.

Acknowledgments

We would like to thank Sam Kaplan and Todd Bown of the University of Alberta for assisting with the prestack-depth-migration processing and wellbore data gathering, respectively. We acknowledge also Colin Zelt and Uri ten Brink for providing copies of rayinvr and RayGUI software, respectively, for implementation of the seismic tomography inversion, and we thank GEDCO Ltd. for access to their VISTA® seismic data processing software via their university support program. The seismic-acquisition field crew included Jawwad Ahmad, Marek Welz, Len Tober, Gabrial Solano, Tiewei He, and Dean Rokosh (University of Alberta); John Pawlowicz, (Alberta Geological Survey, Edmonton); and Alain Plouffe (Geological Survey of Canada, Ottawa). Primary funding for the field programs was initiated by the Geological Survey of Canada and the

Alberta Geological Survey via the Targeted Geoscience Initiative–II programs. The work in this contribution was supported by the National Engineering and Research Council Discovery Grant and the Canada Research Chairs programs to D.R.S.

References

Ahmad, J., 2006, High-resolution seismic and electrical resistivity tomography techniques applied to image and characterize a buried channel: M.S. thesis, University of Alberta.

Ahmad, J., D. R. Schmitt, C. D. Rokosh, and J. G. Pawlowicz, 2009, High resolution seismic and resistivity profiling of a buried Quaternary subglacial valley: Northern Alberta, Canada: Geological Society of America Bulletin, **121**, 1570–1583.

Andriashek, L. D., and N. Atkinson, 2007, Buried channels and glacial-drift aquifers in the Fort McMurray region, NE Alberta: Alberta Energy and Utilities Board, Alberta Geological Survey, EUB/AGS Earth Sciences Report 2007-01.

Auken, E., K. Sorensen, H. Lykke-Andersen, M. Bakker, A. Bosch, J. Gunnink, F. Binot, G. Gabriel, M. Grinat, H. M. Rumpel, A. Steuer, H. Wiederhold, T. Wonik, P. F. Christensen, R. Friborg, H. Guldager, S. Thomsen, B. Christensen, K. Hinsby, F. Jorgensen, I. M. Balling, P. Nyegaard, D. Seifert, T. Sormenborg, S. Christensen, R. Kirsch, W. Scheer, J. F. Christensen, R. Johnsen, R. J. Pedersen, J. Kroger, M. Zarth, H. J. Rehli, B. Rottger, B. Siemon, K. Petersen, M. Kjaerstrup, K. M. Mose, P. Erfurt, P. Sandersen, V. Jokumsen, and S. O. Nielsen, 2009, Buried Quaternary valleys — A geophysical approach: Zeitschrift der Deutschen Gesellschaft für Geowissenschaften, **160**, 237–247.

Baker, G. S., D. W. Steeples, and M. Drake, 1998, Muting the noise cone in near-surface reflection data: An example from southeastern Kansas: Geophysics, **63**, 1332–1338.

Belfer, I., I. Bruner, S. Keydar, A. Kravtsov, and E. Landa, 1998, Detection of shallow objects using refracted and diffracted seismic waves: Journal of Applied Geophysics, **38**, 155–168.

Benjumea, B., J. A. Hunter, J. M. Aylsworth, and S. E. Pullan, 2003, Application of high-resolution seismic techniques in the evaluation of earthquake site response, Ottawa Valley, Canada: Tectonophysics, **368**, 193–209.

Best, M. E., V. M. Levson, T. Ferbey, and D. McConnell, 2006, Airborne electromagnetic mapping for buried Quaternary sands and gravels in northeast British Columbia, Canada: Journal of Environmental and Engineering Geophysics, **11**, 17–26.

Biondi, B., 2003, Equivalence of source-receiver migration and shot-profile migration: Geophysics, **68**, 1340–1347.

Bradford, J. H., L. M. Liberty, M. W. Lyle, W. P. Clement, and S. Hess, 2006, Imaging complex structure in shallow seismic-reflection data using prestack depth migration: Geophysics, **71**, no. 6, B175–B181.

Bradford, J. H., and D. S. Sawyer, 2002, Depth characterization of shallow aquifers with seismic reflection, part II: Prestack depth migration and field examples: Geophysics, **67**, 98–109.

Büker, F., A. G. Green, and H. Horstmeyer, 1998, Shallow seismic reflection study of a glaciated valley: Geophysics, **63**, 1395–1407.

———, 2000, 3-D high-resolution reflection seismic imaging of unconsolidated glacial and glaciolacustrine sediments: Processing and interpretation: Geophysics, **65**, 1395–1407.

Canales, L. L., 1984, Random noise reduction: 54th Annual International Meeting, SEG, Expanded Abstracts, 525–527.

Chambers, J. E., O. Kuras, P. I. Meldrum, R. D. Ogilvy, and J. Hollands, 2006, Electrical resistivity tomography applied to geologic, hydrogeologic, and engineering investigations at a former waste-disposal site: Geophysics, **71**, no. 6, B231–B239.

Clague, J. J., J. L. Luternauer, S. E. Pullan, and J. A. Hunter, 1991, Postglacial deltaic sediments, southern Fraser River delta, British Columbia: Canadian Journal of Earth Sciences, **28**, 1386–1393.

Deen, T., and K. Gohl, 2002, 3-D tomographic seismic inversion of a paleochannel system in central New South Wales, Australia: Geophysics, **67**, no. 5, 1364–1371.

De Iaco, R., A. G. Green, H. R. Maurer, and H. Horstmeyer, 2003, A combined seismic reflection and refraction study of a landfill and its host sediments: Journal of Applied Geophysics, **52**, 139–156.

Fisher, T. G., H. M. Jol, and A. M. Boudreau, 2005, Saginaw Lobe tunnel channels (Laurentide Ice Sheet) and their significance in south-central Michigan, USA: Quaternary Science Reviews, **24**, 2375–2391.

Fradelizio, G. L., A. Levander, and C. A. Zelt, 2008, Three-dimensional seismic- reflection imaging of a shallow buried paleochannel: Geophysics, **73**, no. 5, B85–B98.

Francese, R. G., Z. Hajnal, and A. Prugger, 2002, High-resolution images of shallow aquifers — A challenge in near-surface seismology: Geophysics, **67**, 177–187.

Gabriel, G., R. Kirsch, B. Siemon, and H. Wiederhold, 2003, Geophysical investigation of buried Pleistocene subglacial valleys in northern Germany: Journal of Applied Geophysics, **53**, 159–180.

Greenhouse, J. P., and P. F. Karrow, 1994, Geological and geophysical studies of buried valleys and their fills near

Elora and Rockwood, Ontario: Canadian Journal of Earth Sciences, **31**, 1838–1848.

Henley, D. C., 1999, The radial trace transform: An effective domain for coherent noise attenuation and wave field separation: 69th Annual International Meeting, SEG, Expanded Abstracts, 1204–1207.

Hickin, A. S., B. Kerr, D. G. Turner, and T. E. Barchyn, 2008, Mapping Quaternary paleovalleys and drift thickness using petrophysical logs, northeast British Columbia, Fontas map sheet, NTS 94I: Canadian Journal of Earth Sciences, **45**, 577–591.

Hooke, R. L., and C. E. Jennings, 2006, On the formation of the tunnel valleys of the southern Laurentide ice sheet: Quaternary Science Reviews, **25**, 1364–1372.

Hunter, J. A., S. E. Pullan, R. A. Burns, R. M. Gagne, and R. L. Good, 1984, Shallow seismic reflection mapping of the overburden-bedrock interface with the engineering seismograph — Some simple techniques: Geophysics, **49**, 1381–1385.

Jørgensen, F., H. Lykke-Andersen, P. B. E. Sandersen, E. Auken, and E. Nørmark, 2003a, Geophysical investigations of buried Quaternary valleys in Denmark: An integrated application of transient electromagnetic soundings, reflection seismic surveys and exploratory drillings: Journal of Applied Geophysics, **53**, 215–228.

Jørgensen, F., and P. B. E. Sandersen, 2008, Mapping of buried tunnel valleys in Denmark: New perspectives for the interpretation of the Quaternary succession: Geological Survey of Denmark and Greenland Bulletin, **15**, 33–36.

Jørgensen, F., P. B. E. Sandersen, and E. Auken, 2003b, Imaging buried Quaternary valleys using the transient electromagnetic method: Journal of Applied Geophysics, **53**, 199–213.

Juhlin, C., H. Palm, C. Müllern, and B. Wållberg, 2002, Imaging of groundwater resources in glacial deposits using high-resolution reflection seismics, Sweden: Journal of Applied Geophysics, **51**, 107–120.

Kellett, R., 2007, A geophysical facies description of Quaternary channels in northern Alberta: CSEG Recorder, **32**, no. 10, 49–55.

Lennox, D. H., and V. Carlson, 1967, Geophysical exploration for buried valleys in an area north of Two Hills, Alberta: Geophysics, **32**, 331–362.

Levson, V., 2008, Geology of northeast British Columbia and northwest Alberta: Diamonds, shallow gas, gravel, and glaciers: Canadian Journal of Earth Sciences, **45**, 509–512.

Liner, C. L., 2004, Elements of 3D seismology: PennWell Corporation.

Miller, R. D., D. W. Steeples, and M. Brannan, 1989, Mapping a bedrock surface under dry alluvium with shallow seismic reflections: Geophysics, **54**, 1528–1534.

Montagne, R., and G. L. Vasconcelos, 2006, Extremum criteria for optimal suppression of coherent noise in seismic data using the Karhunen-Loève transform: Physica A, **371**, 122–125.

Morozov, I. B., and A. Levander, 2002, Depth image focusing in traveltime map-based wide-angle migration: Geophysics, **67**, 1903–1912.

Nitsche, F. O., A. G. Green, H. Horstmeyer, and F. Büker, 2002, Late Quaternary depositional history of the Reuss Delta, Switzerland: Constraints from high-resolution seismic reflection and georadar surveys: Journal of Quaternary Science, **17**, 131–143.

ÓCofaigh, C., 1996, Tunnel valley genesis: Progress in Physical Geography, **20,** 1–19.

Ogunsuyi, O., D. Schmitt, and J. Ahmad, 2009, Seismic traveltime inversion to complement reflection profile in imaging a glacially buried valley: 79th Annual International Meeting, SEG, Expanded Abstracts, 3675–3678.

Paulen, R. C., M. M. Fenton, J. A. Weiss, J. G. Pawlowicz, A. Plouffe, and I. R. Smith, 2005, Surficial Geology of the Hay Lake Area, Alberta (NTS 84L/NE): Alberta Energy and Utilities Board, EUB/AGS Map 316, scale 1:100000.

Pawlowicz, J. G., A. S. Hicken, T. J. Nicoll, M. M. Fenton, R. C. Paulen, A. Plouffe, and I. R. Smith, 2004, Shallow gas in drift: Northwestern Alberta: Alberta Energy and Utilities Board, EUB/AGS Information Series 130.

———, 2005a, Bedrock topography of the Zama Lake area, Alberta (NTS 84L): Alberta Energy and Utilities Board, EUB/AGS Map 328, scale 1:250000.

———, 2005b, Drift thickness of the Zama Lake area, Alberta (NTS 84L): Alberta Energy and Utilities Board, EUB/AGS Map 329, scale 1:250000.

Plouffe, A., I. R. Smith, R. C. Paulen, M. M. Fenton, and J. G. Pawlowicz, 2004, Surficial geology, Bassett Lake, Alberta (NTS 84L SE): Geological Survey of Canada, Open File 4637, scale 1:100000.

Pugin, A. J., T. H. Larson, S. L. Sargent, J. H. McBride, and C. E. Bexfield, 2004, Near-surface mapping using SH-wave and P-wave seismic land-streamer data acquisition in Illinois, U. S.: The Leading Edge, **23**, 677–682.

Pugin, A. J.-M., S. E. Pullan, J. A. Hunter, and G. A. Oldenborger, 2009, Hydrogeological prospecting using P- and S-wave landstreamer seismic reflection methods: Near Surface Geophysics, **7**, 315–327.

Pullan, S. E., J. A. Hunter, H. A. J. Russell, and D. R. Sharpe, 2004, Delineating buried-valley aquifers using shallow seismic reflection profiling and grid downhole geophysical logs — An example from southern Ontario, Canada, *in* C. Chen and J. H. Xia, eds., Progress in environmental and engineering geophysics: Proceedings of the International Conference on Environmental and Engineering Geophysics, 39–43.

Roberts, M. C., S. E. Pullan, and J. A. Hunter, 1992, Applications of land-based high resolution seismic reflection analysis to Quaternary and geomorphic research: Quaternary Science Reviews, **11**, 557–568.

Robertsson, J. O. A., K. Holliger, A. G. Green, A. Pugin, and R. De Iaco, 1996, Effects of near-surface waveguides on shallow high-resolution seismic refraction and reflection data: Geophysical Research Letters, **23**, 495–498.

Ronen, J., and J. F. Claerbout, 1985, Surface-consistent residual statics estimation by stack-power maximization: Geophysics, **50**, 2759–2767.

Sanderson, P. B. E., and F. Jørgensen, 2003, Buried Quaternary valleys in western Denmark — Occurrence and inferred implications of groundwater resources and vulnerability: Journal of Applied Geophysics, **53**, 229–248.

Schijns, H., S. Heinonen, D. R. Schmitt, P. Heikkinen, and I. T. Kukkonen, 2009, Seismic refraction traveltime inversion for static corrections in a glaciated shield rock environment: A case study: Geophysical Prospecting, **57**, 997–1008.

Sharpe, D. R., A. Pugin, S. E. Pullan, and G. Gorrell, 2003, Application of seismic stratigraphy and sedimentology to regional hydrogeological investigations: An example from Oak Ridges Moraine, southern Ontario, Canada: Canadian Geotechnical Journal, **40**, 711–730.

Sharpe, D., A. Pugin, S. Pullan, and J. Shaw, 2004, Regional unconformities and the sedimentary architecture of the Oak Ridges Moraine area, southern Ontario: Canadian Journal of Earth Sciences, **41**, 183–198.

Sheriff, R. E., 1980, Nomogram for Fresnel-zone calculation: Geophysics, **45**, 968–972.

Sloan, S. D., D. W. Steeples, and P. E. Malin, 2008, Acquisition and processing pitfall associated with clipping near-surface seismic reflection traces: Geophysics, **73**, no. 1, W1–W5.

Song, J. L., and U. ten Brink, 2004, RayGUI 2.0 — A graphical user interface for interactive forward and inversion ray-tracing: U. S. Geological Survey Open-File Report 2004–1426.

Spitzer, R., F. O. Nitsche, and A. G. Green, 2001, Reducing source-generated noise in shallow seismic data using linear and hyperbolic τ-p transformations: Geophysics, **66**, 1612–1621.

Spitzer, R., F. O. Nitsche, A. G. Green, and H. Horstmeyer, 2003, Efficient acquisition, processing, and interpretation strategy for shallow 3D seismic surveying: A case study: Geophysics, **68**, 1792–1806.

Steeples, D. W., A. G. Green, T. V. McEvilly, R. D. Miller, W. E. Doll, and J. W. Rector, 1997, A workshop examination of shallow seismic reflection surveying: The Leading Edge, **16**, 1641–1647.

Steeples, D. W., and R. D. Miller, 1990, Seismic reflection methods applied to engineering, environmental, and groundwater problems, *in* S. H. Ward, ed., Geotechnical and environmental geophysics, v.1: Review and tutorial: SEG Investigations in Geophysics Series No. 5, 1–30.

———, 1998, Avoiding pitfalls in shallow seismic reflection surveys: Geophysics, **63**, 1213–1224.

Steuer, A., B. Siemon, and E. Auken, 2009, A comparison of helicopter-borne electromagnetics in frequency- and time-domain at the Cuxhaven valley in northern Germany: Journal of Applied Geophysics, **67**, 194–205.

Stoffa, P. L., J. T. Fokkema, R. M. de Luna Freire, and W. P. Kessinger, 1990, Split-step Fourier migration: Geophysics, **55**, 410–421.

Widess, M. B., 1973, How thin is a thin bed?: Geophysics, **38**, 1176–1180.

Wiederhold, H., H. A. Buness, and K. Bram, 1998, Glacial structures in northern Germany revealed by a high-resolution reflection seismic survey: Geophysics, **63**, 1265–1272.

Wiederhold, H., H. M. Rumpel, E. Auken, B. Siemon, W. Scheer, and R. Kirsch, 2008, Geophysical methods for investigation and characterization of groundwater resources in buried valleys: Grundwasser, **13**, 68–77.

Yilmaz, Ö., 2001, Seismic data analysis: Processing, inversion, and interpretation of seismic data: SEG Investigations in Geophysics Series No. 10.

Zelt, C. A., A. Azaria, and A. Levander, 2006, 3D seismic refraction traveltime tomography at a groundwater contamination site: Geophysics, **71**, no. 5, H67–H78.

Zelt, C. A., and R. B. Smith, 1992, Seismic traveltime inversion for 2-D crustal velocity structure: Geophysical Journal International, **108**, 16–34.